

VICTORIA UNIVERSITY
MELBOURNE AUSTRALIA

Preparation and characterization of poly(vinylidene fluoride)/nanoclay nanocomposite flat sheet membranes for abrasion resistance

This is the Accepted version of the following publication

Lai, Chi Yan, Groth, Andrew, Gray, Stephen R and Duke, Mikel (2014)
Preparation and characterization of poly(vinylidene fluoride)/nanoclay
nanocomposite flat sheet membranes for abrasion resistance. *Water
Research*, 57. pp. 56-66. ISSN 0043-1354

The publisher's official version can be found at
<http://www.sciencedirect.com/science/article/pii/S0043135414001912>
Note that access to this version may require subscription.

Downloaded from VU Research Repository <https://vuir.vu.edu.au/24793/>

Preparation and characterization of poly(vinylidene fluoride)/nanoclay nanocomposite flat sheet membranes for abrasion resistance

Chi Yan Lai, Andrew Groth, Stephen Gray and Mikel Duke*

Institute for Sustainability and Innovation, College of Engineering and Science, Victoria University, PO Box 14428, Melbourne, Victoria 8001, Australia

**Tel. +61-3-99197682; Fax +61-3-99197696; email: mikel.duke@vu.edu.au*

Abstract

Membranes with more resilience to abrasive wear are highly desired in water treatment, especially for seawater desalination. Nanocomposite poly(vinylidene fluoride) (PVDF)/nanoclay membranes were prepared by phase inversion and then tested for abrasion resistance. Their material properties were characterized using Fourier-transform infrared spectroscopy (FTIR), thermogravimetric analysis (TGA), tensile testing, scanning electron microscopy (SEM) and energy dispersive spectroscopy (EDS). Nanoclay Cloisite® 15A was utilised as the inorganic nanoparticle incorporated into PVDF. FTIR results showed a shifting of the PVDF crystalline phase from α to β thus indicating that the nanoclay altered the PVDF host material's structure and mechanical properties in terms of stiffness and toughness. Water permeation test showed that nanoclay at low concentration tended to reduce water flux. All nanocomposite membranes, with between 1 wt% and 5 wt% initial nanoclay loading, were more abrasion resistant than the control PVDF membrane. However, the 1 wt% exhibited superior resistance, lasting two times longer than the reference PVDF membrane under the same abrasive condition. The 1 wt% nanoclay membrane appeared less abraded by SEM observation, while also having the greatest tensile strength improvement (from 4.5 MPa to 4.9 MPa). This membrane also had the smallest agglomerated nanoclay particle size and highest toughness compared to the higher nanoclay content membranes. Nanoclays are therefore useful for improving abrasion resistance of PVDF membranes, but optimal loadings are essential to avoid losing essential mechanical properties.

Keywords: Poly(vinylidene fluoride); Nanoclay; Nanocomposite; Ultrafiltration; Abrasion resistance

1. Introduction

Poly(vinylidene fluoride) (PVDF) is one of the most popular materials for commercial membranes, including for water applications such as microfiltration (MF) and ultrafiltration (UF) (Mulder 1996), owing to its excellent thermal stability, chemical resistance and mechanical strength. MF and UF membranes are commonly prepared by immersion precipitation to induce phase inversion (Chen et al. 2006, Mago et al. 2008), and this is the most common technique for commercial fabrication of MF/UF membranes.

Despite the outstanding properties of the material, the durability of existing commercial MF and UF membranes in seawater pretreatment for desalination plants is reduced compared to other municipal water applications. In our previous work (Lai et al. 2014a), we established the case of shortened life expectancy of current pretreatment membranes is due to wear by abrasive particles present in seawater. To protect the membranes, current mitigations include installation of microscreening systems (Voutchkov 2010) and to extract water from deeper and cleaner intakes (Sheldon et al. 1972, Voutchkov 2010). However, these methods are often costly and therefore it is essential to strengthen the membrane itself to reduce the

reliance on mitigation methods and improve the life expectancy of the membranes.

Other than seawater pretreatment, abrasion is also an issue for a number of water treatment processes with membrane filtration. For agricultural use, MF/UF membranes can be used for manure pretreatment to isolate the solid nutrients for fertilizer production. The durability of these membranes is challenged by the presence of abrasive solids including sand and animal hair (Masse et al. 2007). There is also a need for abrasion resistant membranes for certain industrial applications. These include the clarification of glucose syrups and the extraction of fermentation broths where abrasive particles such as the undissolved fermentation residues are present in the feed (Barrett 2004, Bennett 2012). For water and wastewater treatment, membranes with stronger abrasion resistance have potential to treat sources with high turbidity, such as storm water, efficiently while maintaining their integrity. Other than the abrasive particles that are naturally present, powdered activated carbon (PAC) is sometimes added before MF/UF to remove organics as well as odour and taste compounds (Pressdee et al. 2006). This, however, also brought about concerns of PAC causing abrasion to the membrane materials in the long run (Huey et al. 1999). For these applications membranes with stronger abrasion resistance are highly coveted. Membranes made from nanocomposites using nanoclays may be an effective means to achieve this desired strengthening.

Nanoclay, which is of relatively low cost and commercially available (Tjong 2006), has been widely investigated as a nanofiller for nanocomposite materials which have enhanced mechanical properties (Alexandre and Dubois 2000, Causin et al. 2008, Patro et al. 2008, Pavlidou and Papaspyrides 2008, Shah et al. 2004) and abrasion resistance (Dayma et al. 2011, Pan et al. 2010, Peng et al. 2009). These improvements are associated with nanoclay acting as a reinforcing agent as well as changing the PVDF crystalline phase (Peng et al. 2009, Shah et al. 2004). As for the membrane field, improvement in mechanical properties of PVDF/nanoclay flat sheet membranes was also observed previously (Hwang et al. 2011, Lai et al. 2011). Hwang et al (Hwang et al. 2011) demonstrated that a PVDF membrane incorporated with Cloisite® 15A had the highest tensile strength, elongation % and Young's modulus among the four selected commercially available nanoclays. Despite these results demonstrating that PVDF nanocomposite membranes can be effectively produced and show increased strength, little work has been done to explore the effect on abrasion resistance based on our review (Lai et al. 2014b).

Previously, we reported work demonstrating incorporation of nanoclay into PVDF hollow fibre membranes for improved abrasion resistance, and found PVDF nanocomposite membranes lasted up to three times longer than the reference PVDF. The test was conducted using an accelerated abrasion setup, involving shaking hollow fibres in an abrasive slurry and periodically measuring bubble point for skin layer breakthrough (Lai et al. 2014a). Therefore, in this study we have extended the investigation to flat sheet membranes utilising a more conventional technique to measure abrasive wear. Nanocomposite PVDF/Cloisite® 15A flat sheet membranes were fabricated and characterized to determine the concentration of inorganic nanomaterials, as well as mechanical strength, abrasion resistance and water flux.

2. Experimental

2.1. Materials

The powdered PVDF Solef® 1015 used, was a commercial product obtained from Solvay Solexis. The nanoclay used in this study was the commercially available Cloisite® 15A, a natural montmorillonite modified with a quaternary ammonium salt supplied by Southern Clay Products. The organic modifier is a dimethyl, dihydrogenated tallow quaternary ammonium ion as show in Figure 1. The inorganic part of the nanoclay has the general

formula $(\text{Na,Ca})_{0.33}(\text{Al,Mg})_2(\text{Si}_4\text{O}_{10})(\text{OH})_2 \cdot n\text{H}_2\text{O}$. The solvent used was biotech grade ($\geq 99.5\%$) 1-methyl-2-pyrrolidinone (NMP) from Sigma-Aldrich.

Figure 1: Organic modifier used in Cloisite® 15A

2.2. Membrane preparation

Pure PVDF and PVDF/Cloisite® 15A nanocomposite membranes (1 wt%, 3wt% and 5 wt% Cloisite® 15A by weight of PVDF) were prepared by phase inversion. The composition of the synthesis solution is listed in Table 1. PVDF and half of the NMP solvent were stirred at 90°C for 20 hours. The nanoclay was dispersed in the remaining half of NMP by ultrasonication for two hours before mixing with PVDF/NMP solution. The combined solution (or dope) was stirred at 90°C for 3.5 hours followed by 30 minutes of settling to remove excessive air bubbles.

The dope was then coated on a glass substrate with a doctor blade using a gap thickness of 300 μm to form thin films. The membrane was formed by immersion in deionised water at 60°C for 15 minutes, and a skin layer was formed on the membrane surface that was in contact with the quench medium. A portion of the membranes were soaked overnight in a 15 wt% glycerol/water solution in order to preserve their porous structure so they could be stored for later analysis. The membranes were dried in a thermostat cabinet at 30°C for 48 hours.

Table 1. Composition of synthesis solutions

Membranes	PVDF (wt%)	NMP (wt%)	Cloisite® 15A (wt%, by weight of PVDF)
PVDF/15A-0	15	85	0
PVDF/15A-1	14.85	85	1
PVDF/15A-2	14.55	85	3
PVDF/15A-3	14.25	85	5

2.3. Characterization of membranes

2.3.1 Particle size in dispersions

Zetasizer Nano ZS from Malvern Instruments, a Dynamic Light Scattering (DLS) instrument, was used to measure the size of the nanoparticles in the dispersions following ultrasonication. Small samples were taken from the NMP/Cloisite® 15A dispersion and diluted with NMP to about 0.02 wt%, so as to be in the concentration range suitable for particle sizer operation. At least three size distribution measurements were taken for each sample, and the average recorded. No apparent change in particle size was observed during the measurements.

2.3.2 Thermogravimetric analysis

Thermogravimetric analysis (TGA) was performed using a PerkinElmer TGA 7. Cloisite® 15A, PVDF and nanocomposite membrane samples were heated from 50°C to 850°C at a rate of 20°C/min under air at 20 mL/min.

2.3.3 Fourier-transform infrared spectroscopy

Fourier-transform infrared (FTIR) absorption spectra of the membranes were measured with a PerkinElmer Spectrum™ 100 FTIR-ATR to compare the crystalline phases present in the membranes. Based on a previously reported method (Mohammadi et al. 2007, Zhang et al. 2008), the beta fraction (F_β) of a crystalline phase, which is the mass fraction of the β -phase in the PVDF crystal, can be estimated from the absorbance of the characteristic peaks of all crystalline phases and their absorption coefficients as follows:

$$F_\beta = \frac{A_\beta}{\left(\frac{k_\beta}{k_\alpha}\right)A_\alpha + A_\beta} \quad (1)$$

where A_α and A_β are the peak areas of the absorption peaks of α -phase and β -phase at 763 cm⁻¹ and 840 cm⁻¹ respectively. Absorption coefficients of α -phase (k_α) and β -phase (k_β) were taken as 6.1 x 10⁴ cm²/mol and 7.7 x 10⁴ cm²/mol accordingly (Mohammadi et al. 2007, Zhang et al. 2008).

2.3.4 Electron microscopy

Scanning electron microscopy (SEM) of the membrane cross sections were taken with a Nikon/JEOL NeoScope JCM-5000. To obtain the cross section, the membrane sample was first fractured after dipping into liquid nitrogen. Imaging and elemental mapping was performed on the quench side surface of the membranes using a Philips XL30 Field Emission Scanning Electron microscope (FESEM). The samples were mounted on an aluminium stub with double-sided conductive carbon tape. These samples were then carbon coated using a Polaron carbon sputter coater. The thickness of the carbon coating was approximately 240 Å. An accelerating voltage of 10kV was used for the images and X-ray maps. Energy Dispersive Spectroscopy (EDS) x-ray analysis used an Oxford Instruments Pty Ltd system which incorporated an X-Max 80 mm² x-ray detector and Aztec software.

2.3.5 Membrane permeation testing

Pure water flux of the membranes was carried out using deionized water with a Sterlitech CF042 membrane cell which is a laboratory scale cross flow filtration unit. The active membrane area was 42 cm² and the filtration test operated at a constant pressure of 175 kPa. Pure water flux (J_w) was determined using Equation (2)

$$J_w = \frac{Q}{A\Delta t} \quad (2)$$

where Q (L) was the amount of water collected as permeate, A (m²) was the membrane area and Δt (h) was the sampling time. Two samples of each type of membrane were tested.

2.3.6 Mechanical testing

Mechanical properties including elongation at maximum load, tensile strength, Young's modulus and the modulus of toughness of the membranes were measured using an Instron 5500R tensile testing instrument at 20°C. The initial gauge length was 20 mm and the testing speed was 400 mm/min. At least three samples of each type of membrane were tested and the average reported.

2.3.7 Abrasion resistance testing

In our previous study on hollow fibre membrane (Lai et al. 2014a), membranes were made as single loop modules and shaken in silicon carbide slurry with periodic bubble point test to monitor the degree of abrasive wear. Although the setup more closely resembled filtration conditions, it was rather time consuming (more than 20 days) and it would be even more challenging for setting up flat sheet bubble point measurement. As a result, a simpler and more efficient way was proposed for abrasion resistance testing of flat sheet membranes.

Abrasion resistance of the membrane was tested with a Martindale Wear & Abrasion Tester (James H. Heal & Co. LTD) under a pressure of 9 kPa at Standard Textile Testing Conditions ($20 \pm 2^\circ\text{C}$ and $65 \pm 3\%$ RH). All four types of membranes were tested on the same instrument at the same time. The membranes were mounted to holders so that the skin layer of the membrane was contacting the abrasive material underneath. It was essential to ensure this as the skin layer controls the functional separation process and its abrasion resistance is thus more significant than the supporting membrane material. The test was repeated using two different grades of sandpaper made with silicon carbide grain of grit size P1000 and P1200 as the abrasive material. The average particle diameter of abrading materials embedded in P1000 and P1200 sandpaper was $18.3\ \mu\text{m}$ and $15.3\ \mu\text{m}$ respectively. This correlated to the size of common particulates found in seawater such as clay/silt aggregates, which are in the range of $1\text{--}40\ \mu\text{m}$ (McCave 1984). The membrane samples were weighed before and in between the abrasion cycles to record the loss in mass due to abrasive wearing. SEM images of the original and the abraded membrane surface were taken with a Nikon/JEOL NeoScope JCM-5000. An accelerating voltage of 10 kV was used for the images.

3. Results and Discussion

3.1. Thermogravimetric analysis

Figure 2 presents the TGA curves of Cloisite[®] 15A and the four various membranes. All of the membranes exhibited a two-step thermal decomposition that was attributed to break down of the polymer. The first degradation stage occurred between 350°C to 500°C was due to chain-stripping of the polymer backbone (Hirschler 1982). The release of hydrogen and fluoride led to the formation of hydrogen fluoride (Botelho et al. 2008). The second stage, which occurred after 500°C , corresponded to the burn off of the carbonaceous residue (Hirschler 1982). The decomposition curves would be mostly associated with the PVDF material because Cloisite[®] 15A cannot contribute to more than 5% of the total material mass.

Figure 2: TGA thermograms of PVDF composite membranes and Cloisite[®] 15A

As the nanoclay loading increases, the temperature at which the first stage of decomposition commences reduces. Li and Kim (Li and Kim 2008) also noted this weakening in thermal stability in their PVDF/modified clay nanocomposite membranes which have lower activation energy compared to pure PVDF membrane. Small amounts of additives, including silicate and titanate, are able to catalyse the thermal decomposition rate of PVDF (Ameduri 2009). The organic component of Cloisite[®] 15A started to break down at a lower temperature than pure PVDF (i.e. 250°C and 450°C respectively). Despite the small loading in the membrane, the presence of Cloisite[®] 15A caused the decomposition of the composite PVDF/nanoclay membrane to occur at a lower temperature.

The second weight loss step, starting from 450°C to 500°C and ending between 700°C and 800°C , ultimately yields the residual weight left behind after TGA, which is interpreted as the

actual inorganic component of the materials. It was found that 57% of Cloisite® 15A was not combusted after TGA, implying this is the inorganic component of the original nanoclay. This value matches with the weight loss on ignition stated on the supplier's product data sheet of the nanoclay (2008). In all cases, the nanocomposite membranes contained a non-combustible residue that was attributed to the inorganic component of the added nanoclay and increased with the loading. Although it is not seen clearly on Figure 2, it was observed in the pan and measured by the TGA. The results are listed in Table 2 and compared against the original inorganic loading calculated based on the original nanoclay loading in the synthesis solution and the TGA data of the nanoclay.

Table 2: Comparison between original and actual inorganic loading

Material	Original / supplier inorganic loading %	Inorganic residue % (weight % after TGA)	% of nanoclay retained
PVDF/15A-0	0	0.0	-
PVDF/15A-1	0.6	0.1	17
PVDF/15A-2	1.7	0.3	17
PVDF/15A-3	2.9	0.7	24
Cloisite® 15A	57	57	-

Table 2 shows a slight increase in the residual weight percentage which corresponds to an increase in the nanoclay loading. It is observed that the nanoclay content in the final product detected by TGA was only about one fifth of the initial concentration in the dope for all three nanocomposite membranes. This implies some loss during membrane formation and it was likely to occur during the phase inversion process.

3.2. Effect of nanoclay on membrane crystal structure

The FTIR spectra of PVDF and the nanocomposite membranes are shown in Figure 3. The spectra exhibit strong peaks that are associated with different crystalline phases of PVDF. Major peaks were observed at 763 cm^{-1} and 796 cm^{-1} corresponding to the α -phase of PVDF, as well as at 840 cm^{-1} corresponding to the β -phase of PVDF (Shah et al. 2004, Zhang et al. 2008). The α -phase peak intensity decreased in tandem with an increase in the β -phase peak for the nanocomposite membrane samples. This was attributed to a change in PVDF crystal phases during membrane formation, and previous studies have shown that the incorporation of nanoclay can stabilize the formation of β -phase PVDF (Dillon et al. 2006, Peng et al. 2009, Priya and Jog 2003, Shah et al. 2004).

Figure 3. FTIR spectra of the membranes

Table 3 presents the beta fraction, F_β , of the membranes which was calculated using Equation (1) based on the peak areas of the absorption peaks of α -phase and β -phase at 763 cm^{-1} and 840 cm^{-1} respectively. It was observed that the F_β value of the composite membranes increased with nanoclay loading, indicating there was a higher ratio of β -phase crystalline form present in the nanocomposite membranes. This result matches of previous studies (Dillon et al. 2006, Peng et al. 2009, Priya and Jog 2003, Shah et al. 2004), and the reason for the β -phase increase is due to the similarity between the crystal lattice of nanoclay and that of PVDF β -phase (Shah et al. 2004).

Table 3. F_β of membranes

Membrane	F_β
PVDF/15A-0	0.17

PVDF/15A-1	0.45
PVDF/15A-2	0.49
PVDF/15A-3	0.54

Among the five phases of PVDF, namely α , β , γ , δ and ε (Lovinger 1982), α - and β -phase are the most reported and identified (Buonomenna et al. 2007). While α -phase is kinetically favourable owing to a trans-gauche configuration, β -phase has all-trans conformation which is the most thermodynamically stable form (Ameduri 2009). Furthermore, previous studies (Peng et al. 2009, Shah et al. 2004) have identified that shifting from α -phase to β -phase is related to an improvement in abrasion resistance and mechanical properties such as stiffness and toughness in nanocomposite materials.

3.3. Effect of nanoclay on membrane morphology

The cross-section morphology of PVDF and PVDF/Cloisite[®] 15A nanocomposite membranes are presented in Figure 4. All membranes exhibit similar cross section morphology with a thin skin layer on top of small finger-like porous voids on the quench side of the membrane, graduating to the sponge layer on the other side of the membrane (glass-contact side). This asymmetric morphology is common in flat sheet membranes formed by phase inversion (Hwang et al. 2011, Liao et al. 2010, Zhang et al. 2008). The sponge layer is necessary for membrane strength, while the skin layer performs the functional separation. With the progressive incorporation of nanoclay, gradual change in membrane morphology was observed. As the nanoclay content increased, the depth and the width of the finger-like voids increased accordingly. Macrovoid depth can either increase or decrease with surfactant addition (Wang et al. 1998), with the opposite being observed when using different nanoclays (Lai et al. 2014a). The Cloisite[®] 15A chemistry (Figure 1) is, therefore, important in controlling macrovoid formation. In this case, its effect might be explained by an increase in the demixing rate in the phase inversion process as the solid nanoparticles made the synthesis solution thermodynamically less stable (Ma et al. 2012). This brought rapid nucleation from the polymer lean phase and promoted macrovoid formation (Smolders et al. 1992, Sukitpaneemit and Chung 2009).

Figure 4. Cross-sectional morphology of (a) PVDF/15A-0, (b) PVDF/15A-1, (c) PVDF/15A-2 and (d) PVDF/15A-3

Figure 5 displays the water contact side surface morphology of the membranes and the corresponding EDS images of silicon mapping. Since silicon is the most abundant inorganic element present in the nanoclay and it is absent from the PVDF, mapping the silicon distribution in the image provides a good representation of nanoclay dispersion throughout the membrane. The surface of the membranes appeared to be porous in general and as the nanoclay loading increases, it is seen that the intensity of silicon detection also increases. The nanoclay appears to be more finely dispersed for lower loadings and larger agglomerates emerge as the loading increases. Also, the intensity-weighted mean diameter of the Cloisite[®] 15A dispersion of 1.6% nanoparticles in NMP derived from the cumulants analysis by the particle sizer, was found to be 4969 nm. This measurement is comparable to some of the larger particle cluster sizes observed in the EDS mapping images.

Figure 5. Backscattering SEM and silicon mapping images using EDS of membrane quench side surface: (a) PVDF/15A-0, (b) PVDF/15A-1, (c) PVDF/15A-2 and (d) PVDF/15A-3

Table 4 presents the overall thickness and the average thickness of the skin layer for each membrane measured from at least five different locations in the SEM cross-sectional images. While the overall membrane thickness increased with nanoclay loading, there was no statistically significant trend in how the addition of nanoclay impacted the skin layer thickness. Generally the skin layers were approximately 1 μm thick.

Table 4. Overall membrane thickness and average thickness of skin layer

Membrane	Overall Thickness (μm)	Skin layer thickness (μm)
PVDF/15A-0	84 ± 2	1.3 ± 0.1
PVDF/15A-1	91 ± 1	1.5 ± 0.3
PVDF/15A-2	96 ± 1	1.2 ± 0.3
PVDF/15A-3	97 ± 3	0.8 ± 0.1

3.4. Effect of nanoclay on water flux

Figure 6(a) shows water fluxes for the various membranes. The control PVDF membrane gave an average of 5.0 $\text{L}/\text{m}^2\text{h}$ of water flux at 175 kPa transmembrane pressure. The water flux tends to decrease at low nanoclay content but increases to 7.9 $\text{L}/\text{m}^2\text{h}$ as shown by the PVDF/15A-3 membranes. To remove the variation of membrane skin thickness, the product of permeability and skin thickness was plotted against the nanoclay loading in Figure 6(b). It is shown that the addition of nanoclay, especially at lower loading, reduces specific water flux of the material itself once variations in skin layer thickness are accounted for.

The varying flux result suggests that the alteration of membrane formulation with various nanoclay loading alters the membrane morphology that relates to water transport. Besides membrane skin thickness, the contact angle, pore size, tortuosity and skin porosity also influence water permeability and the addition of nanoclay appears to have also influenced these features. It was also noted that these water fluxes were much lower than conventional membranes (Oh et al. 2009). To optimise the water flux, pore-forming agent is needed in the fabrication process. For this paper, only basic PVDF/nanoclay formulation was used so as to scrutinize the impact of the addition of the nanoparticles. The water flux testing provided an indication of the membrane hydraulic performance, which is also an important factor besides aiming to improve the mechanical strength and the abrasion resistance of the membranes.

Figure 6: Impact of nanoclay on (a) membrane water flux (175 kPa) and (b) water flux times skin thickness (specific skin flux)

3.5. Effect of nanoclay on mechanical properties

The test results of mechanical properties including tensile strength and elongation at max load are listed in Table 5. It was observed that nanoclay tended to improve the tensile strength at lower loading and PVDF/15A-1 membrane with 1% initial loading gave the best improvement from 4.5 MPa to 4.9 MPa. Hwang et al (Hwang et al. 2011) also observed improved tensile strength and no apparent change in ductile strength with their PVDF/1wt% Cloisite® 15A flat sheet membrane. As the nanoclay loading increases, elongation at maximum load decreases which indicates the ductile strength of the membrane has been compromised. The decrease in ductility is likely to associate with the increased depth and width of finger-like voids as observed in other studies (Shi et al. 2007, Tsai et al. 2002).

Table 5. Mechanical properties of membranes

Membrane	Tensile strength (MPa)	Elongation at max load (%)
----------	------------------------	----------------------------

PVDF/15A-0	4.5 ± 0.1	222 ± 21
PVDF/15A-1	4.9 ± 0.1	186 ± 7
PVDF/15A-2	4.8 ± 0.1	131 ± 21
PVDF/15A-3	4.5 ± 0.2	104 ± 13

Figure 7 presents Young's modulus and modulus of toughness of PVDF and the composite membranes. It was observed that Young's modulus increased with the nanoclay content, especially for the membranes loaded with 3% and 5% nanoclay (PVDF/15A-2 and PVDF/15A-3) which demonstrates that the addition of nanoclay provides extra stiffness to the polymer matrix. The toughness of a material is defined as the ability of the material to absorb energy up to the point of breakage, and the modulus of toughness is obtained from the area under the stress-strain curve (Agrawal 1988). It was shown that the modulus of toughness reduced as the nanoclay loading increased, showing the composite membranes were less tough than the reference PVDF membrane. These trends could be related to the crystal phase change in PVDF that resulted from incorporation of nanoclay. Nucleation of the fibre-like PVDF β -phase on the faces of individual silicate layers of the nanoclay brings about a structure which is more favourable to plastic flow under applied stress. This results in a more efficient energy-dissipation mechanism in composite membranes, which has been shown in previous PVDF/nanoclay nanocomposite materials studies to delay cracking (Shah et al. 2004). Nanoclay can act as a temporary crosslinker to the polymer chain due to its mobility and this provides localized regions of increased strength and inhibits the development of cracks and cavities (Carretero-Gonzalez et al. 2009, Peng et al. 2009). These changes could cause the material to stiffen and become less tough as the nanoclay loading increases. The PVDF/15A-1 membranes demonstrated the highest tensile strength while other mechanical properties, including ductility, stiffness and toughness, were either maintained or only slightly reduced when compared to all other membranes.

Figure 7. Young's modulus and modulus of toughness of PVDF composite membranes

3.6. Effect of nanoclay on abrasion resistance

Figure 8 presents the weight loss per unit area of each membrane after 200 abrasion cycles using sandpaper with P1000 and P1200 grits. All nanocomposite membranes demonstrated lower weight loss than the reference PVDF membrane in both tests. This implies that the addition of nanoclay enhanced the abrasion resistance and that the nanoparticles provide physical reinforcement to the polymer structure. The result was more sensitive to the coarser grade sandpaper, P1000. The average particle diameter of abrading materials embedded in P1000 sandpaper was $18.3 \mu\text{m}$, compared to $15.3 \mu\text{m}$ in P1200, making it a rougher and more abrasive material. As such, the weight loss of membrane with P1000 was higher overall.

Figure 8. Weight loss per unit area of membrane after 200 abrasion cycles with two different grades of sand paper

The PVDF/15A-1 membrane with 1 wt% initial nanoclay loading gave the smallest weight loss per unit area among the four membranes tested. The PVDF/15A-1 membrane lost 6.2 g/m^2 compared to 14.0 g/m^2 lost by the PVDF membrane. This suggests that the nanocomposite membrane can last two times longer than a conventional unmodified membrane under the same abrasive conditions and would be a candidate material for filtration in more abrasive conditions. In our previous study on hollow fibre membrane (Lai et al. 2014a), the best performing nanocomposite membrane lasted three times longer than the

unmodified membrane. The similar results in both studies infer that the simpler flat sheet sandpaper technique is a reasonable way to test materials for improved abrasion resistance.

SEM images of the quench side membrane surface (skin layer side) before and after abrasion testing with P1000 are shown in Figure 9. Before the test, all membranes appear to have smooth surfaces with no other observable features. After the test, the control PVDF membrane with no nanoclay (PVDF/15A-0) revealed the most worn surface of all four membranes. Nanocomposite membranes appear to be smoother with less pitting in the surface compared to the control membrane, with PVDF/15-1 the least damaged. These observations are comparable to the respective weight loss of the membranes (Figure 8).

Figure 9. SEM images of membrane surface after abrasion testing: (a) PVDF/15A-0, (b) PVDF/15A-1, (c) PVDF/15A-2 and (d) PVDF/15A-3. Original surface is shown as inset in each image.

The improvement of abrasion resistance observed for the nanocomposite membranes could be related to the increased F_β as shown in Table 3. The more abundant β -phase PVDF increases the binding energy between macromolecule chains and improves abrasion resistance as the surface is less likely to peel off, which has been observed in studies of PVDF/clay nanocomposites (Peng et al. 2009). However, it was noted that although PVDF/15-2 and PVDF/15-3 membranes had even higher F_β , they showed greater amounts of weight loss which implies reduced abrasion resistance compared to the PVDF/15A-1 membrane. This weakening could be due to the reduced ductility and toughness as observed earlier (Table 5 and Figure 7) but also owing to increasing size and amount of agglomeration as the nanoclay loading increases. As observed in Figure 5(d), the size of some of the aggregates in PVDF/15A-3 was close to 5 μm , which was greater than the skin layer thickness of the membrane (0.8 μm) (Table 4). Nanoclay agglomeration tends to cause the material to be more readily peeled off during the abrasion process as they induce the stress concentration and cracking (Cai et al. 2003, Peng et al. 2009). As the size and amount of the aggregates increased it started to counter the benefits of the energy dissipation mechanism and increased binding energy in the composite membrane and thus weaker abrasion resistance was observed in membranes with higher loadings. However, our previous study (Lai et al. 2014a) on hollow fibre membranes using different nanoclays showed that the more agglomerated material had stronger abrasion resistance. One reason could be the different surface functionalization of the nanoclay playing a more significant role to the polymer matrix than the actual dispersion in maintaining the abrasion resistance of the membrane. Also, this paper is measuring abrasion by using a standard tribological technique of two surfaces moving in relative motion to each other with one being harder or more abrasive than the other, which is a similar approach of direct contact method used in the literature (Cai et al. 2003, Peng et al. 2009) where they observed nanoclay agglomeration weaken abrasion resistance. This technique uses mass loss as an indicator whereas the slurry abrasion measurement on the hollow fibres uses change in bubble point to determine the extent of abrasion. In addition, flat sheet membrane was used in this study which its entire surface was in contact with the abrasive source. On the other hand, there could be some surface of the hollow fibre may not be directly abraded by the slurry. The effect of nanoclay agglomeration is probably more prominent in flat sheet as being more exposed in abrasion. These differences in the experimental setup could be the reason leading to the different trend observed. Nevertheless, our work has indicated that both overall membrane mechanical properties, and the physical/chemical behaviour of the nanoclays within the PVDF matrix, are tied to the improvement in the abrasion resistance of membranes. This appears to function best at low nanoclay concentration.

4. Conclusions

PVDF/Cloisite[®] 15A nanocomposite flat sheet membranes were fabricated using phase inversion. SEM and EDS images show that the nanoclay was dispersed throughout the membrane and the membrane structure appeared to be altered by the addition of nanoparticles. Nanoclay also promoted a change of the PVDF crystalline phase from α - to β -phase and appeared to reduce water flux at lower loadings. Further investigation with addition of pore-forming agent would be needed to optimize flux for practical use. Nanocomposite membranes exhibited higher tensile strength and stiffness, but lower ductility and toughness. All nanocomposite membranes showed increased resistance to abrasion compared to the reference PVDF material in a simple abrasion testing setup. The PVDF/15A membrane with 1 wt% initial loading demonstrated the highest tensile strength and the strongest abrasion resistance despite the slightly lower toughness compared to reference PVDF material. Nanocomposite PVDF/nanoclay membranes are therefore suitable for improved abrasion resistance in water treatment applications such as desalination pretreatment.

Acknowledgement

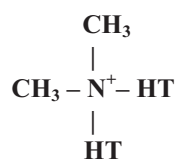
The authors would like to acknowledge the financial support from the Australia Research Council Linkage Project LP100100103, Memcor Products, Evoqua Water Technologies and National Centre of Excellence in Desalination Australia, funded by the Australian Government through the National Urban Water and Desalination Plan. Special thanks to Dr. Marlene Cran and Dr. Bo Zhu from the Victoria University, Dr. Ludovic Dumeé from Deakin University, Mr. John Ward, Mr. Mark Greaves, Mr. Mark Hickey and Ms. Karen Wiener from CSIRO and Dr. Clem Powell from Memcor Products, Evoqua Water Technologies for their advice and assistance on the use of the instruments.

References

- Agrawal, B.K. (1988) Introduction to Engineering Materials, Tata McGraw-Hill.
- Alexandre, M. and Dubois, P. (2000) Polymer-layered silicate nanocomposites: preparation, properties and uses of a new class of materials. Materials Science and Engineering: R: Reports 28(1-2), 1-63.
- Ameduri, B. (2009) From Vinylidene Fluoride (VDF) to the Applications of VDF-Containing Polymers and Copolymers: Recent Developments and Future Trends. Chemical Reviews 109(12), 6632-6686.
- Barrett, S. (2004) Membranes are resistant to abrasion. Membrane Technology 2004(8), 2.
- Bennett, A. (2012) Membrane technology: Developments in ultrafiltration technologies. Filtration + Separation 49(6), 28-33.
- Botelho, G., Lanceros-Mendez, S., Goncalves, A.M., Sencadas, V. and Rocha, J.G. (2008) Relationship between processing conditions, defects and thermal degradation of poly(vinylidene fluoride) in the β -phase. Journal of Non-Crystalline Solids 354(1), 72-78.
- Buonomenna, M.G., Macchi, P., Davoli, M. and Drioli, E. (2007) Poly(vinylidene fluoride) membranes by phase inversion: the role the casting and coagulation conditions play in their morphology, crystalline structure and properties. European Polymer Journal 43(4), 1557-1572.
- Cai, H., Yan, F., Xue, Q. and Liu, W. (2003) Investigation of tribological properties of Al₂O₃-polyimide nanocomposites. Polymer Testing 22(8), 875-882.

- 498 Carretero-Gonzalez, J., Retsos, H., Giannelis, E.P., Ezquerro, T.A., Hernandez, M. and
- 499 Lopez-Manchado, M.A. (2009) Miscibility-dispersion, interfacial strength and nanoclay
- 500 mobility relationships in polymer nanocomposites. *Soft Matter* 5(18), 3481-3486.
- 501 Causin, V., Carraro, M.L., Marega, C., Saini, R., Campestri, S. and Marigo, A. (2008)
- 502 Structure and morphology of solution blended poly(vinylidene fluoride)/montmorillonite
- 503 nanocomposites. *Journal of Applied Polymer Science* 109(4), 2354-2361.
- 504 Chen, J.P., Mou, H., Wang, L.K. and Matsuura, T. (2006) *Advanced Physicochemical*
- 505 *Treatment Processes*. Wang, L.K., Hung, Y.-T. and Shammas, N.K. (eds), pp. 203-259,
- 506 Humana Press Inc., Totowa, NJ.
- 507 Dayma, N., Satapathy, B.K. and Patnaik, A. (2011) Structural correlations to sliding wear
- 508 performance of PA-6/PP-g-MA/nanoclay ternary nanocomposites. *Wear* 271(5-6), 827-836.
- 509 Dillon, D.R., Tenneti, K.K., Li, C.Y., Ko, F.K., Sics, I. and Hsiao, B.S. (2006) On the
- 510 structure and morphology of polyvinylidene fluoride-nanoclay nanocomposites. *Polymer*
- 511 47(5), 1678-1688.
- 512 Hirschler, M.M. (1982) Effect of oxygen on the thermal decomposition of poly(vinylidene
- 513 fluoride). *European Polymer Journal* 18(5), 463-467.
- 514 Huey, B., Heckler, J., Joost, R., Crozes, G. and Gallier, T. (1999) *Combination of Powdered*
- 515 *Activated Carbon and Low Pressure Membrane Filtration: A Process Alternative for SRP*
- 516 *Water Treatment*, American Water Works Association, Denver, CO, USA.
- 517 Hwang, H.-Y., Kim, D.-J., Kim, H.-J., Hong, Y.-T. and Nam, S.-Y. (2011) Effect of nanoclay
- 518 on properties of porous PVDF membranes. *Transactions of Nonferrous Metals Society of*
- 519 *China* 21(Supplement 1), 141-147.
- 520 Lai, C.Y., Groth, A., Gray, S. and Duke, M. (2011) Investigation of the dispersion of
- 521 nanoclays into PVDF for enhancement of physical membrane properties. *Desalination and*
- 522 *Water Treatment* 34(1-3), 251-256.
- 523 Lai, C.Y., Groth, A., Gray, S. and Duke, M. (2014a) Enhanced abrasion resistant
- 524 PVDF/nanoclay hollow fibre composite membranes for water treatment. *Journal of*
- 525 *Membrane Science* 449(0), 146-157.
- 526 Lai, C.Y., Groth, A., Gray, S. and Duke, M. (2014b) Nanocomposites for Improved Physical
- 527 Durability of Porous PVDF Membranes. *Membranes* 4(1), 55-78.
- 528 Li, H. and Kim, H. (2008) Thermal degradation and kinetic analysis of PVDF/modified MMT
- 529 nanocomposite membranes. *Desalination* 234(1-3), 9-15.
- 530 Liao, C., Zhao, J., Yu, P., Tong, H. and Luo, Y. (2010) Synthesis and characterization of
- 531 SBA-15/poly (vinylidene fluoride) (PVDF) hybrid membrane. *Desalination* 260(1-3), 147-
- 532 152.
- 533 Lovinger, A.J. (1982) *Development in Crystalline Polymers*. Basset, D.C. (ed), Applied
- 534 Science Publishers, London.
- 535 Ma, Y., Shi, F., Wang, Z., Wu, M., Ma, J. and Gao, C. (2012) Preparation and
- 536 characterization of PSf/clay nanocomposite membranes with PEG 400 as a pore forming
- 537 additive. *Desalination* 286(0), 131-137.
- 538 Mago, G., Kalyon, D.M. and Fisher, F.T. (2008) Membranes of polyvinylidene fluoride and
- 539 PVDF nanocomposites with carbon nanotubes via immersion precipitation. *Journal of*
- 540 *Nanomaterials* 2008(1).
- 541 Masse, L., Massé, D.I. and Pellerin, Y. (2007) The use of membranes for the treatment of
- 542 manure: a critical literature review. *Biosystems Engineering* 98(4), 371-380.
- 543 McCave, I.N. (1984) Size spectra and aggregation of suspended particles in the deep ocean.
- 544 *Deep Sea Research Part A. Oceanographic Research Papers* 31(4), 329-352.
- 545 Mohammadi, B., Yousefi, A.A. and Bellah, S.M. (2007) Effect of tensile strain rate and
- 546 elongation on crystalline structure and piezoelectric properties of PVDF thin films. *Polymer*
- 547 *Testing* 26(1), 42-50.

- Mulder, M. (1996) Basic principles of membrane technology, Kluwer Academic, Dordrecht ; Boston.
- Oh, S.J., Kim, N. and Lee, Y.T. (2009) Preparation and characterization of PVDF/TiO₂ organic-inorganic composite membranes for fouling resistance improvement. *Journal of Membrane Science* 345(1-2), 13-20.
- Pan, B., Xing, Y., Zhang, C. and Zhang, Y. (2010) Study on erosion wear behavior of PDCPD/MMT nanocomposite. *Advanced Materials Research* 123-125, 231-234.
- Patro, T.U., Mhalgi, M.V., Khakhar, D.V. and Misra, A. (2008) Studies on poly(vinylidene fluoride)-clay nanocomposites: Effect of different clay modifiers. *Polymer* 49(16), 3486-3499.
- Pavlidou, S. and Papaspyrides, C.D. (2008) A review on polymer-layered silicate nanocomposites. *Progress in Polymer Science* 33(12), 1119-1198.
- Peng, Q.-Y., Cong, P.-H., Liu, X.-J., Liu, T.-X., Huang, S. and Li, T.-S. (2009) The preparation of PVDF/clay nanocomposites and the investigation of their tribological properties. *Wear* 266(7-8), 713-720.
- Pressdee, J.R., AWWA Research Foundation, American Water Works Association and Van Der Hoek, J.P. (2006) Integration of Membrane Filtration Into Water Treatment Systems, Awwa Research Foundation/American Water Works Association/IWA Pub.
- Priya, L. and Jog, J.P. (2003) Polymorphism in intercalated poly(vinylidene fluoride)/clay nanocomposites. *Journal of Applied Polymer Science* 89(8), 2036-2040.
- Shah, D., Maiti, P., Gunn, E., Schmidt, D.F., Jiang, D.D., Batt, C.A. and Giannelis, E.P. (2004) Dramatic Enhancements in Toughness of Polyvinylidene Fluoride Nanocomposites via Nanoclay-Directed Crystal Structure and Morphology. *Advanced Materials* 16(14), 1173-1177.
- Sheldon, R.W., Praksh, A. and W. H. Sutcliffe, J. (1972) The size distribution of particles in the ocean. *Limnology and Oceanography* 17(3), 327-340.
- Shi, L., Wang, R., Cao, Y., Feng, C., Liang, D.T. and Tay, J.H. (2007) Fabrication of poly(vinylidene fluoride-co-hexafluoropropylene) (PVDF-HFP) asymmetric microporous hollow fiber membranes. *Journal of Membrane Science* 305(1-2), 215-225.
- Smolders, C.A., Reuvers, A.J., Boom, R.M. and Wienk, I.M. (1992) Microstructures in phase-inversion membranes. Part 1. Formation of macrovoids. *Journal of Membrane Science* 73(2-3), 259-275.
- Southern Clay Products (2008) Cloisite® 15A Typical Physical Properties Bulletin, Gonzales, Texas.
- Sukitpaneevit, P. and Chung, T.-S. (2009) Molecular elucidation of morphology and mechanical properties of PVDF hollow fiber membranes from aspects of phase inversion, crystallization and rheology. *Journal of Membrane Science* 340(1-2), 192-205.
- Tjong, S.C. (2006) Structural and mechanical properties of polymer nanocomposites. *Materials Science and Engineering: R: Reports* 53(3-4), 73-197.
- Tsai, H.A., Hong, M.J., Huang, G.S., Wang, Y.C., Li, C.L., Lee, K.R. and Lai, J.Y. (2002) Effect of DGDE additive on the morphology and pervaporation performances of asymmetric PSf hollow fiber membranes. *Journal of Membrane Science* 208(1-2), 233-245.
- Voutchkov, N. (2010) Considerations for selection of seawater filtration pretreatment system. *Desalination* 261(3), 354-364.
- Wang, D.-M., Lin, F.-C., Wu, T.-T. and Lai, J.-Y. (1998) Formation mechanism of the macrovoids induced by surfactant additives. *Journal of Membrane Science* 142(2), 191-204.
- Zhang, M., Zhang, A.-Q., Zhu, B.-K., Du, C.-H. and Xu, Y.-Y. (2008) Polymorphism in porous poly(vinylidene fluoride) membranes formed via immersion precipitation process. *Journal of Membrane Science* 319(1-2), 169-175.



Where HT is Hydrogenated Tallow (~65% C18; ~30% C16; ~5% C14)

Anion: Chloride

Figure 1. Organic modifier used in Cloisite® 15A

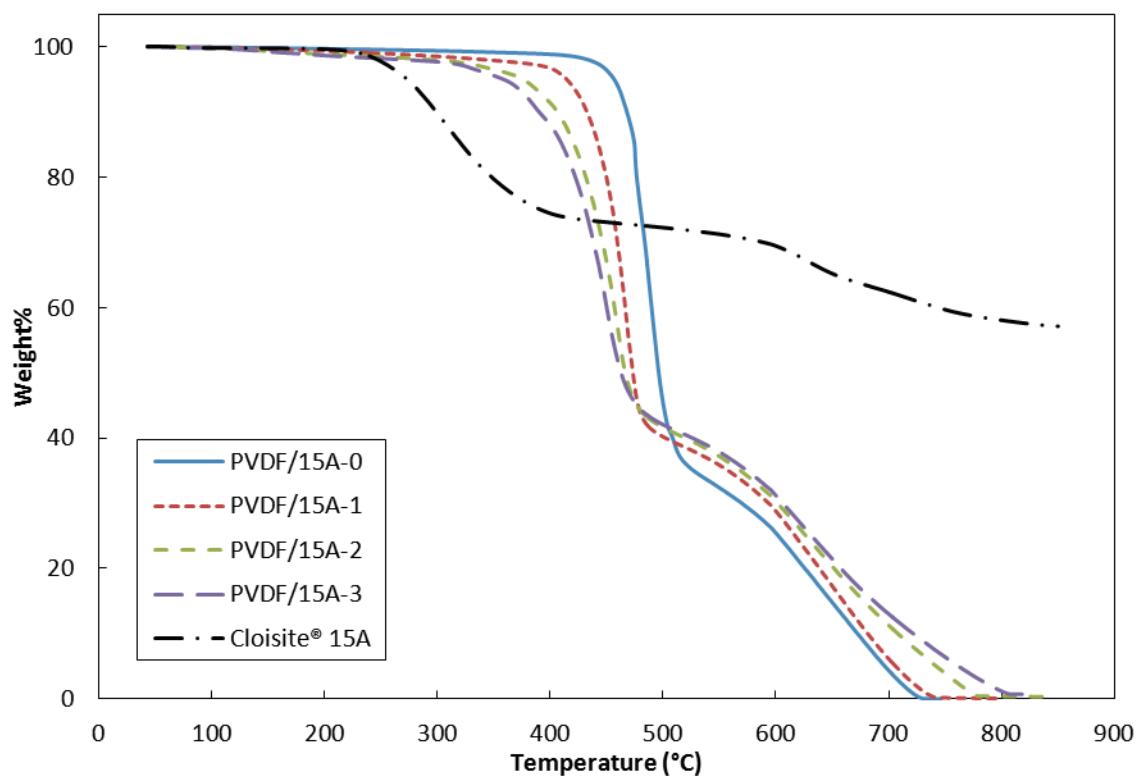


Figure 2. TGA thermograms of PVDF composite membranes and Cloisite® 15A

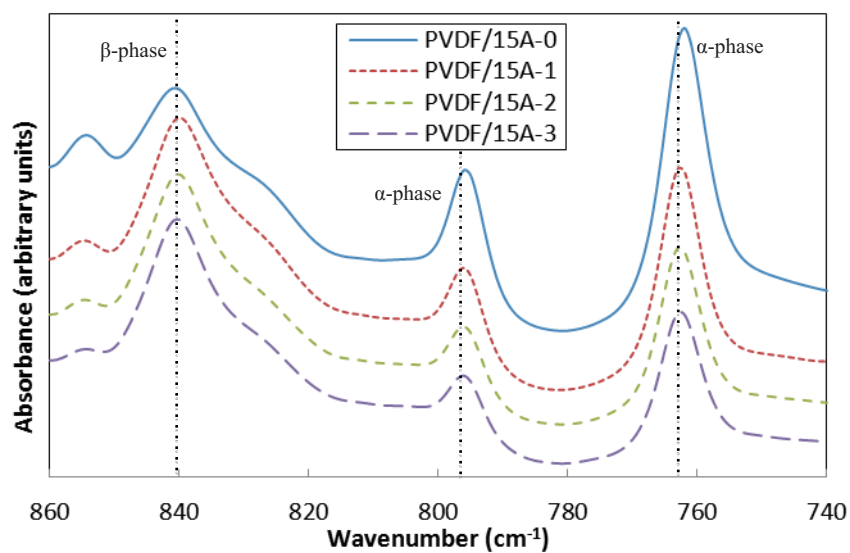


Figure 3. FTIR spectra of the membranes

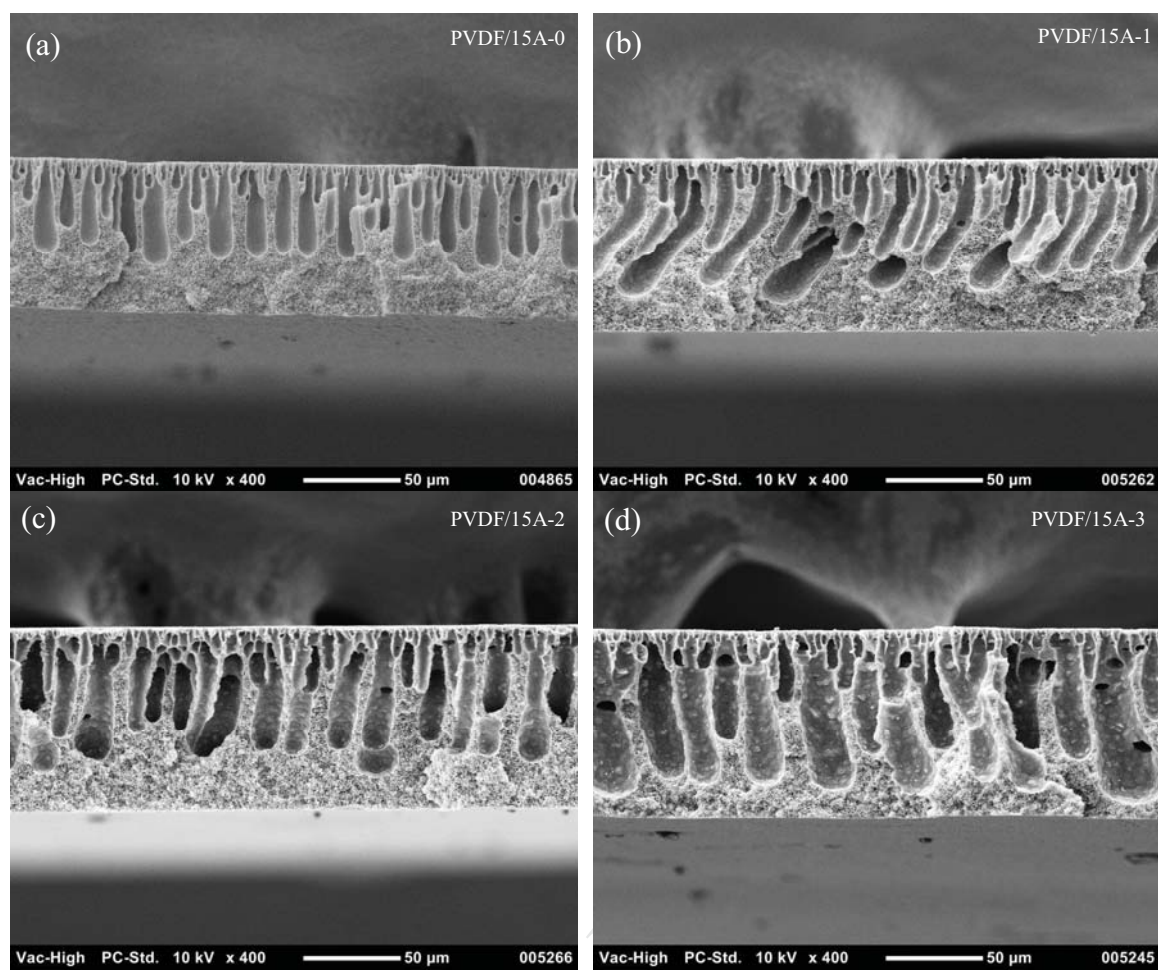


Figure 4. Cross-sectional morphology of (a) PVDF/15A-0, (b) PVDF/15A-1, (c) PVDF/15A-2 and (d) PVDF/15A-3

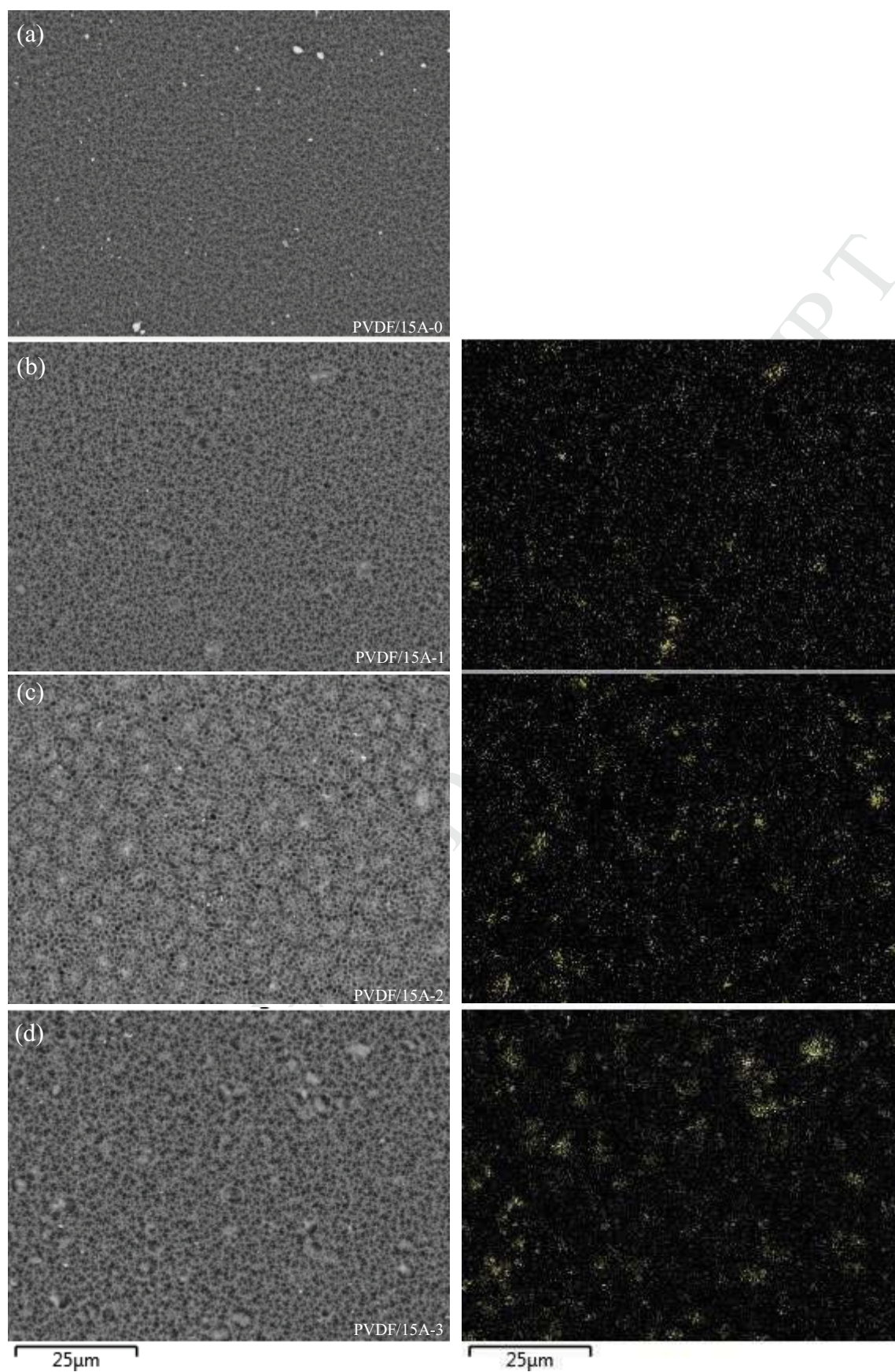


Figure 5. Backscattering SEM and silicon mapping images using EDS of membrane quench side surface: (a) PVDF/15A-0, (b) PVDF/15A-1, (c) PVDF/15A-2 and (d) PVDF/15A-3

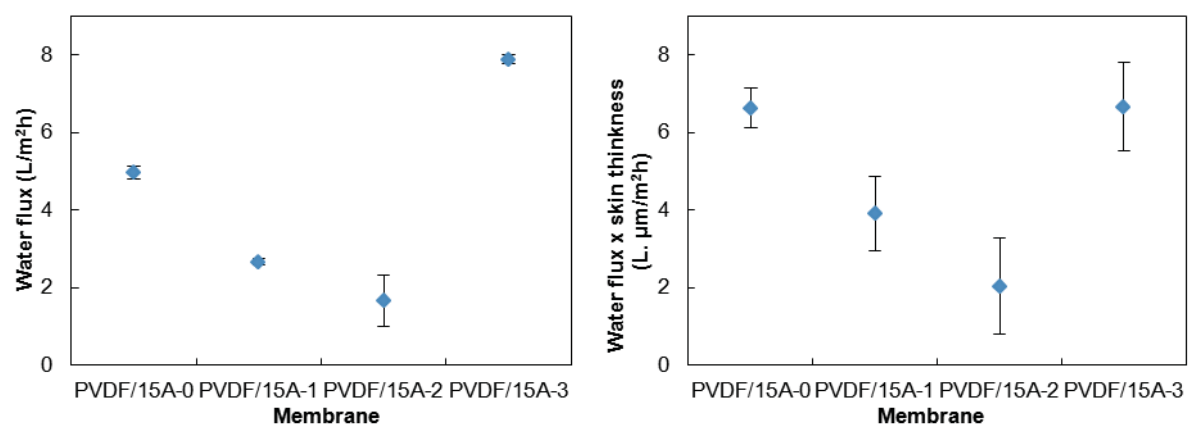


Figure 6. Impact of nanoclay on (a) membrane water flux (175 kPa) and (b) water flux times skin thickness (specific skin flux)

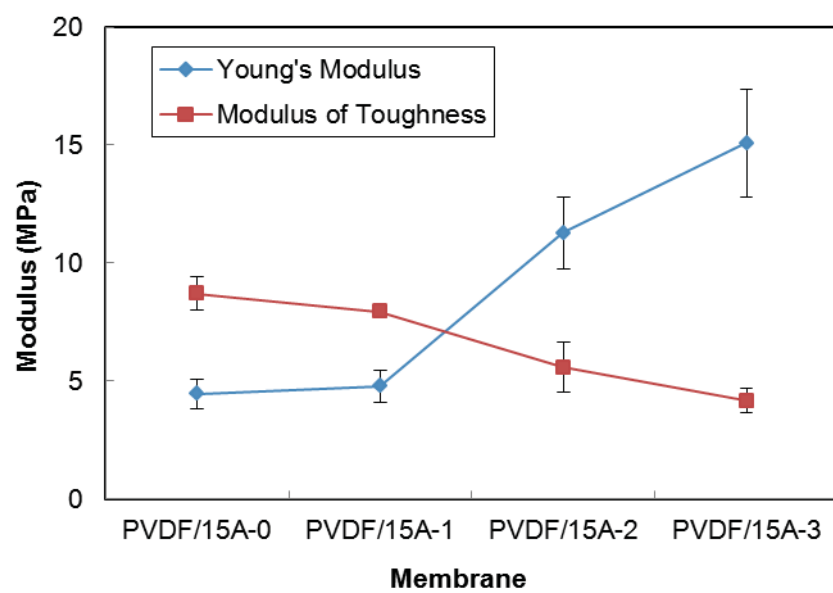


Figure 7. Young's modulus and modulus of toughness of PVDF composite membranes

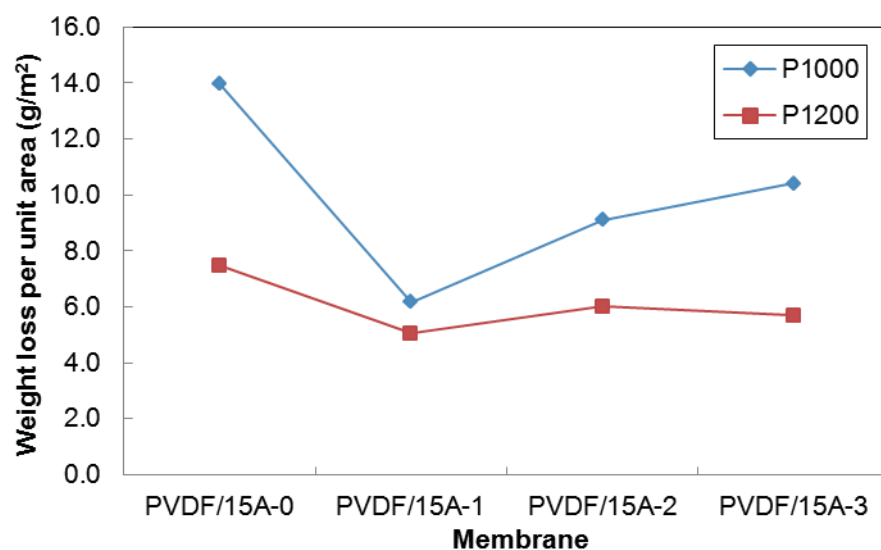


Figure 8. Weight loss per unit area of membrane after 200 abrasion cycles with two different grades of sand paper

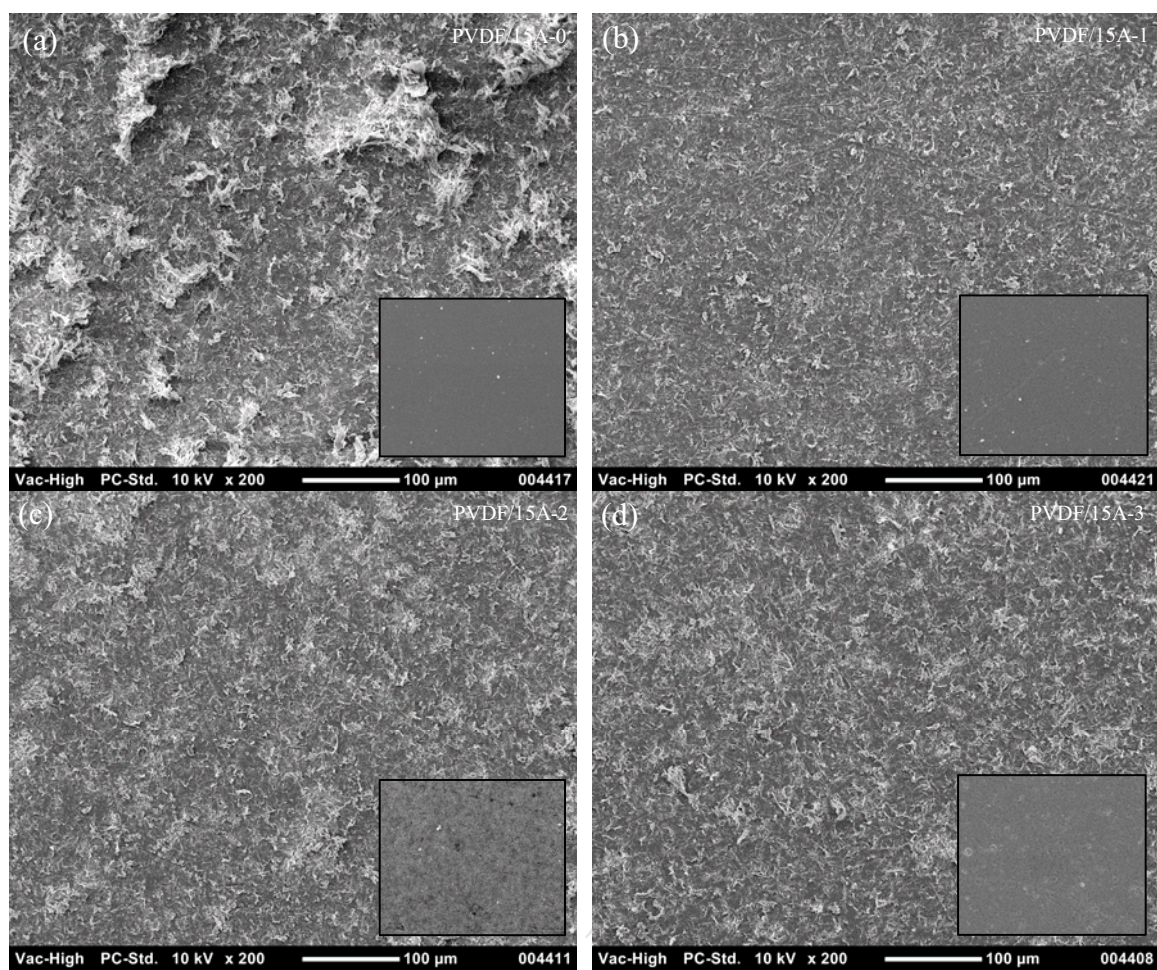


Figure 9. SEM images of membrane surface after abrasion testing: (a) PVDF/15A-0, (b) PVDF/15A-1, (c) PVDF/15A-2 and (d) PVDF/15A-3. Original surface is shown as inset in each image.

Highlight

- Abrasion of membranes is a significant issue in water treatment
- PVDF/nanoclay flat sheet membranes were prepared by phase inversion.
- Nanoclay promoted PVDF β -phase formation and enhanced abrasion resistance.
- Membrane with 1% initial loading had best tensile strength and abrasion resistance.